Soft Matter

PAPER

View Article Online
View Journal | View Issue

Cite this: *Soft Matter*, 2017, 13, 7922

Chain dynamics and nanoparticle motion in attractive polymer nanocomposites subjected to large deformations†

Erkan Senses,*[ab] Madhusudan Tyagi,[ab] Bharath Natarajan,[c] Suresh Narayanan[d] and Antonio Faraone*[a]

Received 20th May 2017,
Accepted 28th September 2017

DOI: 10.1039/c7sm01009e

rsc.li/soft-matter-journal

The effect of large deformation on the chain dynamics in attractive polymer nanocomposites was investigated using neutron scattering techniques. Quasi-elastic neutron backscattering measurements reveal a substantial reduction of polymer mobility in the presence of attractive, well-dispersed nanoparticles. In addition, large deformations are observed to cause a further slowing down of the Rouse rates at high particle loadings, where the interparticle spacings are slightly smaller than the chain dimensions, *i.e.* in the strongly confined state. No noticeable change, however, was observed for a lightly confined system. The reptation tube diameter, measured by neutron spin echo, remained unchanged after shear, suggesting that the level of chain–chain entanglements is not significantly affected. The shear-induced changes in the interparticle bridging reflect the slow nanoparticle motion measured by X-ray photon correlation spectroscopy. These results provide a first step for understanding how large shear can significantly affect the segmental motion in nanocomposites and open up new opportunities for designing mechanically responsive soft materials.

1. Introduction

Polymer nanocomposites (PNCs) with attractive polymer–nanoparticle (NP) interactions, involving a confined interfacial layer ($\approx$1 nm thick) close to the particle surface[1] and a bulk-like matrix with a larger interphase region around the fillers, are of great interest for their applicative purposes.[2] The 'bound' polymer layer in PNCs has received significant attention in the polymer physics community[3–8] due to its distinct structure and dynamics with respect to a neat matrix, which ultimately determine the bulk rheological properties of the composite materials.[9–11] The NPs in such systems are often reported to disperse individually,[4,12–15] enabling the investigation of interfacial effects on the rheological properties without contribution from particle percolation.

The dynamic mechanical response of PNCs has been investigated in oscillatory shear.[16] At a small amplitude, composites usually behave more solid-like with improved elastic modulus relative to a more liquid-like particle-free matrix homopolymer. This 'gel-like' behavior is typical of PNCs with well-dispersed NPs and has been attributed to a network effect of the particles bridged by the irreversibly adsorbed polymer layer around nanoparticles.[15,17] Increasing strain amplitude at constant frequency results in a transition from the linear (constant moduli) to nonlinear (decreasing/increasing moduli) regime at a critical amplitude, γ_C. The onset of nonlinearities appears to be highly dependent on particle concentration and occurs at much smaller values in nanocomposites compared to the neat homopolymer. This phenomenon, which has significant relevance in polymer and nanocomposite processing, is known as the Payne effect[18] in rubber filled systems and is commonly attributed to the desorption of bound chain segments and the release of trapped entanglements,[16] enhanced lifetime of the glassy layer on nanoparticles,[8] as well as to the breakdown of the filler network structure.[19] NP structural reorganization under large shear has been studied in non-attractive systems, as the polymer and particles are likely to self-assemble or aggregate.[20–23]

In this work, we present neutron scattering investigations on isotopically labeled polymers to study how the segmental and the reptation dynamics of a model attractive system, poly(ethylene oxide)–SiO_2 NPs, change after a large shear deformation. While the NP microstructure can easily be probed by electron microscopy or X-ray scattering techniques, the hierarchical nature of polymer structure and dynamics requires simultaneously accessing both

[a] *NIST Center for Neutron Research, National Institute of Standards and Technology Gaithersburg, MD 20899-8562, USA. E-mail: antonio.faraone@nist.gov*
[b] *Department of Materials Science and Engineering, University of Maryland College Park, MD 20742-2115, USA. E-mail: erkan@umd.edu*
[c] *Materials Measurement Laboratory, National Institute of Standards and Technology Gaithersburg, MD 20899, USA*
[d] *Advanced Photon Source, Argonne National Laboratory, Argonne, IL 60439, USA*

† Electronic supplementary information (ESI) available: QENS data at $Q = 3.6$ nm^{-1}, SANS profiles of contrast matched samples and XPCS results. See DOI: 10.1039/c7sm01009e

length and time scales where the microscopic chain motions take place. Dynamic neutron scattering techniques, namely Quasi-Elastic Neutron Scattering (QENS) and Neutron Spin Echo (NSE), uniquely afford such a possibility. Our results show that the pinning and bridging in PNCs with attractive polymer–NP interactions can be effectively changed with an external deformation and have direct consequences in bulk rheology as well as slow nanoparticle motion in polymer melts that is probed by X-ray photon correlation spectroscopy.

2. Experimental details

Hydrogenated PEO (hPEO) (M_w: 35 kg mol^{-1}, M_w/M_n = 1.08) and deuterated PEO (dPEO) (M_w: 35 kg mol^{-1}, M_w/M_n = 1.09) were supplied by Polymer Source Inc. and dried further under vacuum at 90 °C for 12 h. Colloidal silica nanoparticles (average diameter of 48 nm with size polydispersity of 0.3) in methyl ethyl ketone were supplied by Nissan Chemical America and used as received. The PNCs were prepared by casting the sonicated mixture of 48% hPEO, 52% dPEO and the desired number of particles in acetonitrile on Teflon cups followed by drying at ambient temperature for 12 h and annealing for 2 days under vacuum at 90 °C. At 48/52 h/d PEO ratio, the Small Angle Neutron Scattering (SANS) from the particles is eliminated at the intermediate and high Q (see ESI†). The particle-free d/h PEO was prepared using an identical protocol. The additional low-Q scattering in particle filled polymers has been the topic of much discussion. Common hypotheses include polymer voids,[24] SLD mismatch,[5] large scale composition fluctuations of H/D polymers,[25] or different affinities of D and H chains on surfaces.[26,27] Regardless, in the region of NSE Q-range used (2 nm^{-1} > Q > 0.8 nm^{-1}), the coherent signal is predominantly due to the single-chain form factor of PEO, thus allowing the study of the collective single-chain dynamics of the polymer matrix.

The fracture cross-sections of the various silica–PEO nanocomposites were imaged using a FEI Helios dual-beam focused ion beam (FIB)/scanning electron microscope (SEM). The samples were scanned using an electron beam at a voltage of 3 kV, a current of 200 pA, and imaged using a highly-sensitive, high-performance Ion Conversion and Electron (ICE) secondary electron (SE) detector. A working distance of 3 mm was used.

The QENS experiments were performed using the NG2-High-Flux Backscattering spectrometer (HFBS)[28] at the NIST Center for Neutron Research (NCNR) on sample films of ≈100 μm thick after at least 2 h of thermal equilibration at the measurement temperature, T = 363 K. Doppler shifted neutrons with incident wavelength of 0.627 nm provide a dynamic range of ±11 μeV (with FWHM resolution of 0.8 μeV, as determined from a measurement of the same sample at 4 K). The backscattered data are collected over a wave vector range Q = 2.5 nm^{-1} to 17.5 nm^{-1}. An empty cell was used to subtract the background scattering and the detector efficiency was corrected using Vanadium data.

The collective single-chain PEO dynamics were obtained using the NGA-NSE spectrometer at NCNR. The measurements were performed at 423 K using a wavelength of λ = 0.8 nm and 1.1 nm ($\Delta\lambda/\lambda$ = 0.15) for Fourier times up to 100 ns and a wave vector range of Q = 0.8 nm^{-1} to 2.0 nm^{-1}. The samples were sealed in Al-cans in a Helium environment. Charcoal was used to obtain the NSE instrumental resolution. Both HFBS and NSE data were reduced and analyzed using DAVE software packages.[29]

The rheology experiments were performed at 363 K on a strain-controlled ARES-G2 (TA instruments) rheometer equipped with a 25 mm cone and plate fixtures with 0.1 rad cone angle and in a nitrogen environment.

The X-ray photon correlation spectroscopy experiments were performed using a photon energy of 11 keV on beamline 8-ID-I at the Advanced Photon Source at Argonne National Laboratory. The samples were equilibrated at desired temperatures for 15 min prior to measurements. The normalized intensity–intensity autocorrelation function, $g_2(Q,t)$, was obtained over the wave vector range 0.03 nm^{-1} < Q < 0.20 nm^{-1} and analyzed at 36 discrete Q values. Five subsequent measurements were performed to ensure that the NP dynamics were identical (see Fig. S4, ESI†) and the results were reported from the last measurements.

3. Results and discussion

Fig. 1 shows the SEMs of well-dispersed NPs in PEO samples with a NP mass fraction of 0.15 (7.8% by volume), 0.30 (17% by volume) and 0.45 (28% by volume), hereafter referred to as 15%, 30% and 45%, respectively. The good dispersion is due to favorable interaction between the oxygen atom on PEO and hydroxyl groups on NPs, which forms a physically bound polymer layer on NPs forming a steric protection of NPs against aggregation. The good dispersion of these NPs in PEO was also verified in a series of previous studies.[6,14] The average face-to-face distances between the NPs were estimated from the random particle distribution, ID = $2R[(2/\pi\phi)^{1/3} - 1]$ with ϕ being the particle volume fractions. The ratios of the face-to-face inter-particle distances relative to the end-to-end distance of 35 kg mol^{-1} PEO (R_{ee} ≈ 18.3 nm)[30] are estimated to be ≈2.97, 1.30 and 0.84 for the 15%, 30% and 45% NPs, respectively. With the highest particle loading, 45%, the polymer is slightly below the critical geometric confinement limit (ID/R_{ee} = 1), whereas 30% is lightly confined. The nanoparticles remain well dispersed after deformation (as shown on Fig. 1 and Fig. S5, ESI†): the dynamical changes discussed later are not due to changes in particle structure.

We apply oscillatory strain, $\gamma(\omega,t) = \gamma_0 \sin(\omega t)$, to deform the samples and obtain the elastic (G') and the viscous (G'') moduli from the stress response, $\sigma(\omega,t) = \sigma_0 \sin(\omega t + \delta)$, that are in-phase ($G' = \sigma_0/\gamma_0 \cos\delta$) and out-of phase ($G'' = \sigma_0/\gamma_0 \sin\delta$) with the applied strain, respectively. At a fixed frequency, ω = 100 rad s^{-1}, the transition from the linear to nonlinear regime was observed in strain-sweeps (Fig. 2a). The Payne effect due to NPs is clearly observed as the onset between the linear and the nonlinear regime shifts to lower γ_0 with increasing particle loading. The frequency sweeps at the small (linear) deformation regime in Fig. 2b show the transition of PEO PNCs from liquid to gel-like behavior as evidenced by the deviations

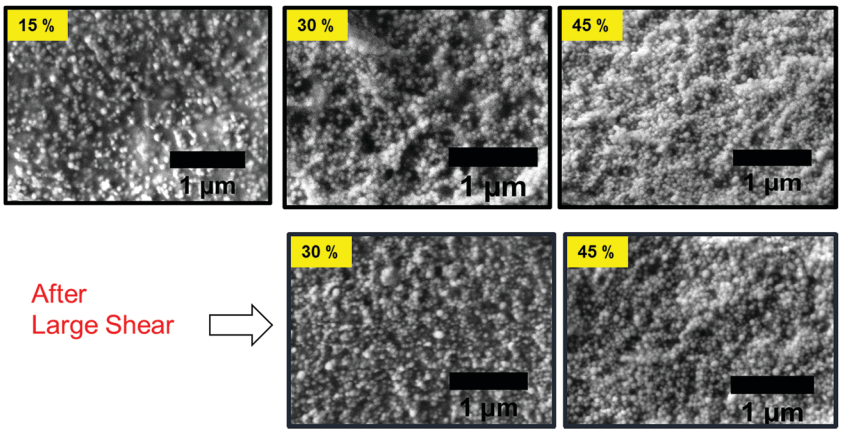

Fig. 1 SEM images of as-cast PNCs with 15%, 30% and 45% (by mass) SiO_2 NPs and PNCs with 30% and 45% NPs after large shear-recovery protocol.

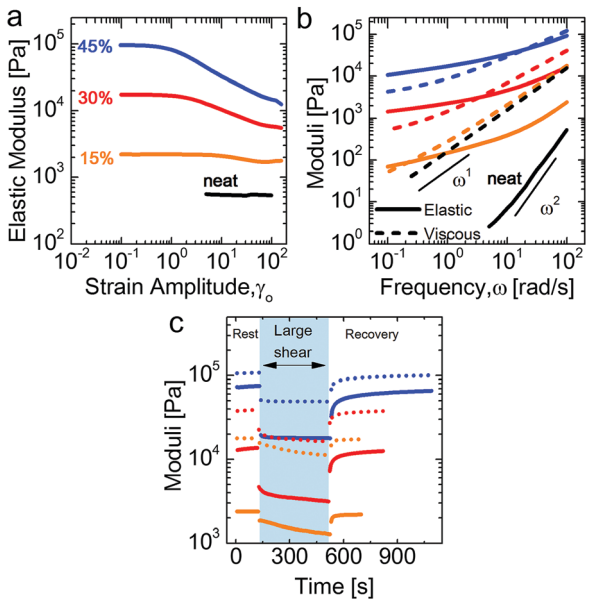

Fig. 2 (a) Strain amplitude sweeps at a deformation frequency of 100 rad s^{-1}. (b) Frequency-dependent dynamic moduli at small amplitude deformation. (c) Evolution of moduli at rest, during large amplitude shear (see the text for details) and recovery.

from scaling of moduli $G' \propto \omega^2$ and $G'' \propto \omega^1$ typical of the neat polymer in the terminal flow regime. Such gel-like responses in well-dispersed attractive PNCs are due to a percolation of the particle network mediated by polymer adsorbed on NPs.[15,17] Our interest in the current work is in the nonlinear deformation regime. We therefore applied a large oscillatory strain in the nonlinear regime at ω = 100 rad s^{-1} and at strain amplitudes γ_0 = 1 for 15% and 30% PNCs and γ_0 = 0.8 for PNC with 45% loading to match the relative distance from the onset of nonlinearities, $(\gamma_0 - \gamma_C)/\gamma_C$, in the 30% and 45% samples. Fig. 2c shows the elastic and viscous moduli evolution during initial linear (small strain) deformation followed by ≈4800 cycles of large shear. The samples were then subjected to small strain to observe the re-equilibration and recovery of the moduli. Note that the moduli decreased upon application of large shear as suggested by the amplitude sweep in Fig. 2a; however, the rates of decrease remarkably get smaller with increasing NP loading and become nearly zero for the 45% loading. Also, the time to recover the moduli after large shear is extended with increasing NP loading, presumably due to slow kinetics. The samples after large shear and recovery were quenched to −70 °C and brought to room temperature after deformation to suppress crystallization of PEO at room temperature. We note that the concentrations larger than 45% were highly reinforced and become practically solid-like, making them difficult to deform at large shear. We, therefore, focused on the samples with 30% and 45% NPs to perform our neutron scattering investigation to represent lightly confined $(ID/R_{ee} > 1)$ and confined states $(ID/R_{ee} < 1)$ and used a less concentrated 15% sample to examine the nanoparticle motion in XPCS in the absence of interparticle interactions.

In a typical dynamic neutron scattering experiment, the double differential scattering cross-section, *i.e.* the probability that neutrons are scattered into a solid angle with an energy change, is measured and related to the incoherent and coherent dynamic structure factors, $S_{inc}(Q,\omega)$ and $S_{coh}(Q,\omega)$. Incoherent scattering is related to the spatial correlations of the same atom at different times and gives the self-motion, while coherent scattering is due to spatial correlations between different atoms at different times and gives the collective motion. We investigated the local segmental dynamics at 363 K (well above the glass-transition temperature of PEO, $T_g \approx 210$ K) using a neutron backscattering spectrometer. Owing to the large incoherent scattering cross-section of H compared with coherent and incoherent cross-sections of all other atoms within the composites, the quasi-elastic scattering measured in the backscattering experiments originates mostly from the self-motion of H atoms through energy change of the scattered neutrons corresponding to time scales ranging from 100 ps to ≈2 ns. The HFBS data are collected over a range of wave vectors Q = 2.5 nm^{-1} to 17.5 nm^{-1}. As the Rouse dynamics is due to segmental motions, the relevant length scale is between the segment length, and the entanglement tube diameter ($d \approx 5.3$ nm). Furthermore, the Rouse model is applicable only to short (unentangling) polymers or short time-scale motions in long (entangling) polymers in the melt state.

At 400 K for PEO, the Rouse model applies up to a time scale on the order of nanoseconds as shown in a previous study.[31] Brodeck *et al.*[32] also showed that the Rouse motion of PEO is captured in backscattering up to Q = 6 nm^{-1}. We, therefore, chose to analyze the QENS spectra at Q = (3.6 and 4.7) nm^{-1}. At these Q values, the residual coherent contribution to the scattering can be estimated from the SANS curves to be 30% and 20%, respectively (see ESI† for details). This, however, does not affect our comparison between the different samples because the SANS pattern, and thus the relative weight of the coherent and incoherent contributions, does not change between the different samples or after shear (Fig. S1, ESI†). Moreover, the line shape of the coherent contribution can be estimated on the basis of the obtained results (see ESI,† for details). At Q = 2.5 nm^{-1}, the signal is dominated by the coherent contribution by 50%; therefore, we excluded this lowest Q value from the analysis of the self-dynamic structure factor discussed below.

Fig. 3a and b compare the normalized self-dynamic structure factors, $S_{inc}(Q,\omega)$, obtained for the neat PEO and the 30% and 45% PNCs at Q = 4.7 nm^{-1} at 363 K. It is clear that the neat PEO relaxes faster as its spectra are broader compared to those of the PNCs. To further quantify, one can calculate the mean-square displacements (MSD), $\langle r^2(t)\rangle$, by Fourier transformation of the dynamic structure factor into the time domain. The intermediate self-dynamic structure factor is related to the MSD by the Gaussian approximation,[33]

$$S_{self}(Q,t) = \exp\left[-Q^2/6\langle r^2(t)\rangle\right] \quad (1)$$

In the framework of the Rouse model, the MSD is related to the elementary Rouse parameter, Wl^4, by $\langle r^2(t)\rangle = \sqrt{4Wl^4t/\pi}$, where $W = 3kT/(\zeta l^2)$, with ζ being the monomeric friction coefficient and the segment length, l. For the segment length, the monomer length value l = 0.58 nm[34] might be assumed, given the extreme flexibility of PEO and the observation that the Rouse model describes the experimental QENS results up to very high Q values. Fig. 3c shows the MSDs against the Rouse scaling, $\sqrt{t}$. For t < 1 ns and displacements smaller than ≈0.8 nm, linear dependence prevails allowing determination of the Rouse rates, Wl^4, from the slopes of the fitting lines (Table 1). The QENS spectra for Q = 3.6 nm^{-1} are presented in the ESI.† Alternatively, to validate our conclusions against dependencies on the method of analysis, QENS data can be fitted in the energy domain; the trends after shear are similar to those obtained from the Rouse analysis in the time domain (see ESI† for representative fits and discussion).

The Wl_{PEO}^4 (T = 363 K) value for the neat polymer is similar to our earlier result,[6] but ≈2 times smaller than what was estimated from the literature data for PEO.[31] This discrepancy can partially be explained by the contribution from the coherent scattering, which can be estimated to result in an apparent decrease of the Wl^4 parameter by ≈60% and ≈40% at Q = 3.6 nm^{-1} and 4.7 nm^{-1}, respectively (see ESI† for the detailed calculation). The slowing down of segmental dynamics is consistent with previous results on PNCs with attractive fillers resulting in extended relaxation times of bound chains in NPs as well as on

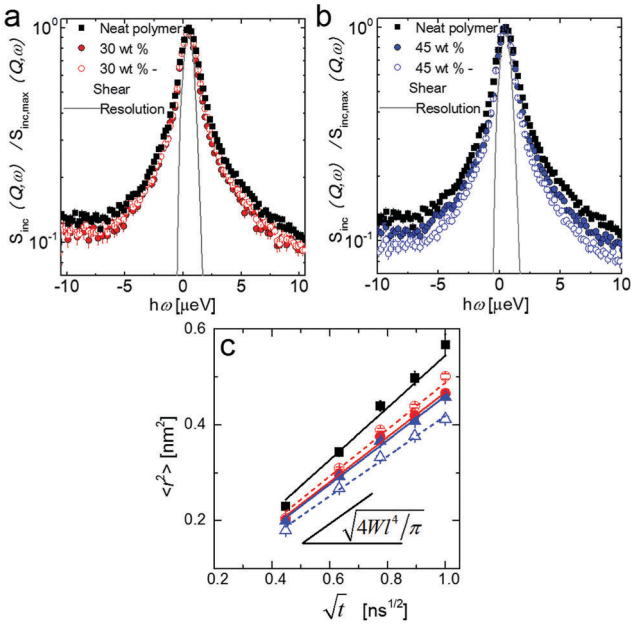

Fig. 3 Self-dynamics from QENS-Rouse motion. Incoherent dynamic structure factors obtained in neutron backscattering for the (a) 30% and (b) 45% samples. Neat polymer data (black squares) are given for comparison. (c) Mean-square displacement (MSD) obtained from the Inverse-Fourier transformed data at Q = 4.7 nm^{-1} plotted on Rouse scaling ($\sqrt{t}$). The solid and dashed lines are the best fits to the unsheared and sheared samples, respectively. All the data shown in this figure are for Q = 4.7 nm^{-1}. See ESI† for Q = 3.6 nm^{-1} data.

Table 1 Characteristic Rouse rates (Wl^4) of PEO at T = 363 K determined as the average of the results from the self-intermediate scattering function $S(Q,t)$ at Q = 3.6 nm^{-1} and Q = 4.7 nm^{-1}. Similar trends can be obtained by a fitting in the energy domain (see ESI)

Sample	Wl^4 [nm^4 ns^{-1}]
Neat PEO	0.182 ± 0.006
PEO-30% by weight SiO_2	0.140 ± 0.005
PEO-30% by weight SiO_2-SHEAR	0.138 ± 0.004
PEO-45% by weight SiO_2	0.129 ± 0.003
PEO-45% by weight SiO_2-SHEAR	0.106 ± 0.003

dynamically asymmetric polymer blends imposing heterogeneous mobility.[6,13,31,35,36] Most interesting is the narrowing of the spectra of 45% PNC (Fig. 3b) after large shear, suggesting an additional ≈18% decrease in the Rouse rate with respect to the unsheared composite. In contrast, no significant change is observed for the 30% sample after large shear. This suggests that the confinement may play a significant role in modifying the interfacial polymer dynamics. In the strong confinement regime, ID/R_{ee} < 1 (45% loading in our case), practically all the chains are bound to a particle surface and the bound chains overlap. These overlapped interfacial chains have to be deformed for the composites to flow. The loop and tails of the chains can therefore be deformed and more surface contacts may be created during shear. This is consistent with an earlier prediction for confined polymers under large shear.[37,38] In the lightly confined system, ID/R_{ee} > 1 (30% loading in our case), it is more likely that the free chains disentangle from the bound chains and allow material to flow

without significantly distorting the interfacial chain packing. This is consistent with stiffening behavior after shear,[12] which is enhanced when the chains are near confinement.

Decrease in segmental relaxation rates implies extended terminal relaxation as the reptation time (τ_d), the time for a chain to escape its original tube, is related to Wl^4 by $\tau_d = 3N^3l^2/W\pi^2d^2$, where d is the reptation tube diameter. Essentially, the long-time chain motion is determined by both the microscopic time scale, Wl^4, and the length scale of chain–chain entanglements, *i.e.* the reptation tube diameter, d. We directly measured the reptation tube diameter of PEO in a zero-average contrast matched 45% PNC sample using neutron spin-echo spectroscopy (NSE) before and after large shear. Thus, we obtained single-chain dynamic structure factor in time domain, $S(Q,t)$ (Fig. 4). For long entangling polymers, the $S(Q,t)$ shows an initial fast decay due to the Rouse motion of chain segments within the tube and then reaches a Q-dependent plateau at longer times due to self-confinement (entanglements). The long-time behavior is well described by the de Gennes equation:[39]

$$\frac{S(Q,t)}{S(Q,0)} = \left[1 - \exp\left(-\frac{Q^2d^2}{36}\right)\right] S^{\text{local}}(Q,t) + \exp\left(-\frac{Q^2d^2}{36}\right) S^{\text{esc}}(Q,t) \quad (2)$$

where $S^{\text{local}}(Q,t) = \exp(t/\tau_0)\text{erfc}\left(\sqrt{t/\tau_0}\right)$ is the local reptation within the tube with characteristic time scale $\tau_0 = 36/(Wl^4Q^4)$. $S^{\text{esc}}(Q,t)$ is the long-time creeping of the chain out of its original tube and $S^{\text{esc}}(Q,t) = 1$ for the motions probed by NSE in this work as $t_{\text{NSE}} \ll \tau_R(\approx 1\ \mu s)$. The long-time plateau level is determined by $\exp(-Q^2d^2/36)$. $Wl^4 = 2.17\ \text{nm}^4\ \text{ns}^{-1}$ at 423 K was estimated using the Vogel–Fulcher–Tammann relationship for the neat PEO,[40,41] $Wl^4(T) \propto \exp[-B/(T - T_0)]$ with $B = 1090$ K and $T_0 = 155$ K. The only remaining free parameter, the reptation tube diameter, d, was obtained from global-fitting of eqn (1) to the data. Since eqn (1) does not account for the initial unrestricted Rouse motion at short times, fitting was applied for $t > 50$ ns to obtain the tube sizes and the curve was extrapolated to shorter times (Fig. 4).

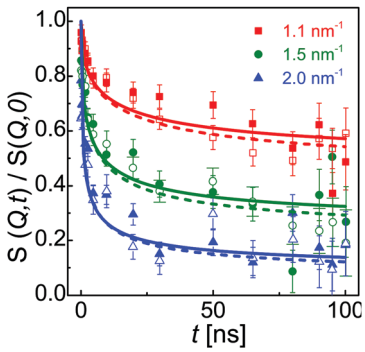

Fig. 4 Collective dynamics-reptation motion. Single-chain dynamic structure factor of the PEO nanocomposite with 45% SiO_2 before shear (filled symbols) and after shear (open symbols) at $T = 423$ K. The curves are the global fit results from the de Gennes equation[39] with elementary Rouse rate, $Wl^4 = 1.55\ \text{nm}^4\ \text{ns}^{-1}$ for PNC without large shear and $Wl^4 = 1.27\ \text{nm}^4\ \text{ns}^{-1}$ for PNC after large shear. The data are fit for $t > 50$ ns and then the curves were extrapolated for shorter times.

The tube sizes of PEO in PNC with 45% SiO_2 loading before and after large shear were found to differ by $\approx 7\%$ ($d_{\text{NC,before-shear}} = 4.8 \pm 0.2$ nm and $d_{\text{NC,after-shear}} = 5.2 \pm 0.2$ nm); however, this difference is within the margins of error. Previous NSE studies on PNCs[42] reported that the apparent tube size in PNCs starts decreasing in the presence of repulsive NPs above the percolation of spherical particles, which occurs at $\phi \approx 31\%$ where the chains feel the geometric confinement.[43] Our system 45% (22% by volume) sample falls below this regime where the geometric confinement is not effective; therefore, it is not surprising that we do not observe a significant change in d. Also, the systems reported in the above-mentioned works consist of repulsive polymer–NP interactions as opposed to the attractive system we present in this study. The mechanical response in nanocomposites is a combined effect of polymer and nanoparticles. In attractive systems with dispersed nanoparticles, it originates from chain pinning on nanoparticle surfaces and the bridging of the nanoparticles through the bound polymer. This results in increasing elastic modulus at much lower particle concentrations where the tube size does not necessarily change significantly.

Slowing down segmental dynamics without changing the entanglement density after shear has important implications for bulk rheological properties as well as for the transport properties of NPs in a polymer melt. The elastic properties of the polymers are mainly determined by the level of entanglements providing a transient network. One would expect an unchanged plateau modulus for a homopolymer since its value is determined by the tube diameter, $G_N^0 = 4R_e^2\rho RT/(5M_wd^2)$. However, in the presence of attractive fillers, the additional polymer mediated, long-lived particle network can also contribute to the elasticity.[15,17] This component is dominant as shown in Fig. 2b (notice the difference between the composites and neat samples) before and after shear. Upon application of large shear, the bridges between NPs may break but they can also reform in the quiescent state after large shear. The comparison of the linear frequency sweeps before the large shear and the recovery, shown in Fig. 5, shows that the crossover frequencies shift to lower values in the sheared samples – the composites behave more liquid-like after shear. Note that the crossovers observed are indicative of soft network-like behavior and differ from the crossover between the terminal relaxation and the rubbery regime, which is out of the time-range probed by bulk rheology. Such a fluidization effect may originate from either a decrease of entanglement density in the bulk of the matrix or weaker bridges forming after large shear. The unchanged tube diameters of the PEO determined by NSE before and after large shear rule out the bulk disentanglements of the matrix chains; it is more likely that the fluidization is caused by de-bridging of particles after large shear.

Bulk rheology typically has no spatial resolution and estimates average viscoelastic properties of the material at macroscopic time scales (compared to (sub)nanosecond dynamics measured by QENS). It is clear from the QENS data from the unsheared samples that the overall segmental relaxation rate is decreased with increased particle loading, suggesting that reduced rates are due to interfacial chain adsorption. The narrowing of the QENS

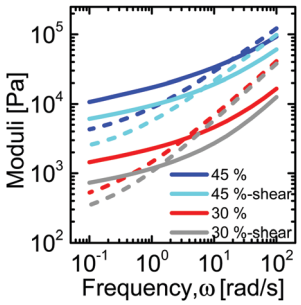

Fig. 5 Linear frequency sweeps on the shear and rested samples shown on Fig. 1e. The crossover moduli shift to lower frequencies – the sheared samples are less gel-like after shear. The solid lines and dashed lines are for elastic and viscous moduli, respectively.

spectra after shear indicates an increase in the pinned segment population. This would result in decreased fractions of loop and tails,[44–46] which are primarily responsible for interparticle bridging. The plateau modulus, therefore, may decrease after shear and the composite can behave more liquid-like (as shown in Fig. 5) after shear, although the number of segments that are directly in contact with the surface increases significantly (causing an overall reduction of Rouse rates).

Further evidence is found by examining the slow motion of NPs as they are largely influenced by the microscale viscosity of the polymer matrix.[47–49] We performed XPCS experiments on the 15% PNC sample before and after shear-recovery (in Fig. 2c) at length scales ranging from ≈20 nm to ≈200 nm. The time scales of the particle motions are between 10 ms and 100 s, and therefore comparable to the time scale probed in linear frequency sweeps ($1/\omega \approx$ 10 ms to 10 s). In the concentrated regime, *e.g.* at 30% (by mass) and higher, the particle motion can be influenced by the local caging effects[50,51] and the XPCS results are not directly connected to the macroscopic rheology. Hence, these data would not likely provide clear insight on the chain dynamics, which is the main theme of this work. The intensity–intensity autocorrelation function is related to the intermediate scattering function (ISF), $f(Q,t)$, as $g_2(Q,t) = 1 + A[f(Q,t)]^2$ where A is the instruments' Siegert factor and t is the delay time. $f(Q,t)$is fit to a stretched or compressed exponential for decay, $f(Q,t) = \exp[-(t/\tau)^{\beta}]$, with τ being the relaxation time and β the stretching/compressing exponent.

The representative correlation functions and fits are shown in the inset of Fig. 6. The relaxation of our large NPs in a liquid polymer is simple exponential with $\beta \approx 1$ and τ scales with Q between ballistic (Q^{-1}) and diffusive (Q^{-2}) motions, making it difficult to estimate the exact viscosity numbers. Regardless, the relaxation time of NPs at all length scales probed by XPCS decreased 5-fold after large shear and recovery compared to the as-cast state, suggesting that the NPs locally experience significantly lower viscosity after large deformation. This is in good agreement with the fluidization of the composites after large shear and the proposed mechanism of weaker bridges forming after shearing due to enhanced chain pinning at the nanoparticle surface.

Finally, we would like to note that different shear rates and/or flow types, *e.g.* steady flow *vs.* oscillatory flow, or deformation protocols, *e.g.* multiple shear-rest cycles, may promote other mechanisms.[12] It is also noteworthy that the structure of the bound polymer depends highly on the polymer molecular weight.[4,52,53]

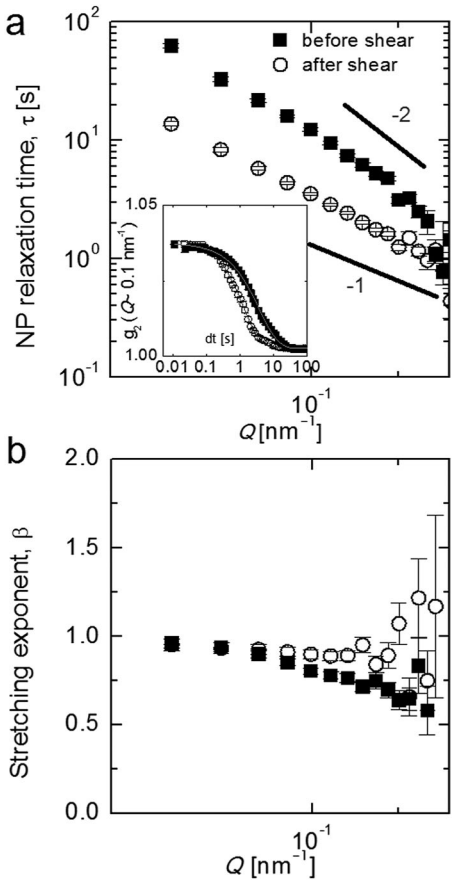

Fig. 6 (a) Wave vector dependent nanoparticle relaxation time (τ) obtained from the fittings of stretched exponential function to the autocorrelation functions (representative profile is given in the inset for $Q \approx 0.1$ nm^{-1}). (b) Corresponding stretching exponent, β, as a function of Q.

4. Conclusions

We have employed dynamic neutron scattering on attractive PEO–silica nanocomposites and studied the effect of large shear deformation on the segmental and collective dynamics of the polymer. Quasi-elastic neutron backscattering measurements showed a reduction of polymer mobility in the presence of attractive, well-dispersed nanoparticles. In the case of a lightly confined system where the face-to-face distance of NPs exceeds greatly the chain size, there was practically no difference between the unsheared and sheared states in terms of Rouse rates. However, a further slowing down of segmental relaxation after large shear was observed at a high particle concentration, when the face-to-face particle separation is smaller than the chain size. At larger length scale, the tube diameter of the polymer in this nanocomposite remained unaffected. Slow nanoparticle motion probed by XPCS shows a substantial decrease in local viscosity (at length scale 20 nm to 200 nm) suggesting strong fluidization likely due to weaker bridges forming after large shear. We believe

that our first direct experimental observation of segmental dynamics and reptation motion on sheared samples provide new insight into the bridging/de-bridging effect of the polymer layer adsorbed on the NP and will stimulate more experimental and theoretical work on these important phenomena.

Author contributions

ES prepared the samples and performed the rheological measurements. BN obtained the electron microscopy images. AF and ES performed the NSE experiments. ES and MT performed the backscattering experiments. ES, AF and SN performed the XPCS experiments. The manuscript was written through contributions of all the authors. All the authors have given approval to the final version of the manuscript.

Conflicts of interest

There are no conflicts to declare.

Acknowledgements

This work utilized facilities supported in part by the National Science Foundation under Agreement No. DMR-1508249 and used resources of the Advanced Photon Source, a U.S. Department of Energy (DOE) Office of Science User Facility operated for the DOE Office of Science by Argonne National Laboratory under Contract No. DE-AC02-06CH11357. The research was performed in part at the NIST Center for Nanoscale Science and Technology (CNST). We are thankful to The Security Technologies Group for the use of the rheometer. Certain trade names and company products are identified in order to specify adequately the experimental procedure. In no case does such identification imply recommendation or endorsement by the National Institute of Standards and Technology, nor does it imply that the products are necessarily the best for the purpose.

References

1 S. Gong, Q. Chen, J. F. Moll, S. K. Kumar and R. H. Colby, *ACS Macro Lett.*, 2014, **3**, 773–777.
2 S. K. Kumar, B. C. Benicewicz, R. A. Vaia and K. I. Winey, *Macromolecules*, 2017, **50**, 714–731.
3 P. J. Griffin, V. Bocharova, L. R. Middleton, R. J. Composto, N. Clarke, K. S. Schweizer and K. I. Winey, *ACS Macro Lett.*, 2016, **5**, 1141–1145.
4 S. Cheng, A. P. Holt, H. Wang, F. Fan, V. Bocharova, H. Martin, T. Etampawala, B. T. White, T. Saito and N.-G. Kang, *Phys. Rev. Lett.*, 2016, **116**, 038302.
5 S. Sen, Y. Xie, S. K. Kumar, H. Yang, A. Bansal, D. L. Ho, L. Hall, J. B. Hooper and K. S. Schweizer, *Phys. Rev. Lett.*, 2007, **98**, 128302.
6 E. Senses, A. Faraone and P. Akcora, *Sci. Rep.*, 2016, **6**, 29326.
7 S. E. Harton, S. K. Kumar, H. Yang, T. Koga, K. Hicks, H. Lee, J. Mijovic, M. Liu, R. S. Vallery and D. W. Gidley, *Macromolecules*, 2010, **43**, 3415–3421.
8 S. Merabia, P. Sotta and D. R. Long, *Macromolecules*, 2008, **41**, 8252–8266.
9 B. Pukánszky, *Eur. Polym. J.*, 2005, **41**, 645–662.
10 M. Krutyeva, A. Wischnewski, M. Monkenbusch, L. Willner, J. Maiz, C. Mijangos, A. Arbe, J. Colmenero, A. Radulescu and O. Holderer, *Phys. Rev. Lett.*, 2013, **110**, 108303.
11 N. Jiang, M. K. Endoh, T. Koga, T. Masui, H. Kishimoto, M. Nagao, S. K. Satija and T. Taniguchi, *ACS Macro Lett.*, 2015, **4**, 838–842.
12 E. Senses and P. Akcora, *Macromolecules*, 2013, **46**, 1868–1874.
13 G. P. Baeza, C. Dessi, S. Costanzo, D. Zhao, S. Gong, A. Alegria, R. H. Colby, M. Rubinstein, D. Vlassopoulos and S. K. Kumar, *Nat. Commun.*, 2016, **7**, 11368.
14 E. Senses, A. Isherwood and P. Akcora, *ACS Appl. Mater. Interfaces*, 2015, **7**, 14682–14689.
15 Q. Chen, S. Gong, J. Moll, D. Zhao, S. K. Kumar and R. H. Colby, *ACS Macro Lett.*, 2015, **4**, 398–402.
16 S. Sternstein and A.-J. Zhu, *Macromolecules*, 2002, **35**, 7262–7273.
17 G. P. Baeza, C. Dessi, S. Costanzo, D. Zhao, S. Gong, A. Alegria, R. H. Colby, M. Rubinstein, D. Vlassopoulos and S. K. Kumar, *Nat. Commun.*, 2016, **7**, 11368.
18 A. Payne and G. Kraus, *Interscience*, New York, 1965, vol. 25.
19 P. Cassagnau, *Polymer*, 2003, **44**, 2455–2462.
20 E. Senses and P. Akcora, *J. Polym. Sci., Part B: Polym. Phys.*, 2013, **51**, 764–771.
21 E. Senses, Y. Jiao and P. Akcora, *Soft Matter*, 2014, **10**, 4464–4470.
22 J. Moll, S. K. Kumar, F. Snijkers, D. Vlassopoulos, A. Rungta, B. C. Benicewicz, E. Gomez, J. Ilavsky and R. H. Colby, *ACS Macro Lett.*, 2013, **2**, 1051–1055.
23 Y. Chen, J. Liu, L. Liu, H. Han, Q. Xu and X. Qian, *RSC Adv.*, 2017, **7**, 8898–8907.
24 K. Nusser, S. Neueder, G. J. Schneider, M. Meyer, W. Pyckhout-Hintzen, L. Willner, A. Radulescu and D. Richter, *Macromolecules*, 2010, **43**, 9837–9847.
25 A.-C. Genix, M. Tatou, A. Imaz, J. Forcada, R. Schweins, I. Grillo and J. Oberdisse, *Macromolecules*, 2012, **45**, 1663–1675.
26 A. Banc, A.-C. Genix, C. Dupas, M. Sztucki, R. Schweins, M.-S. Appavou and J. Oberdisse, *Macromolecules*, 2015, **48**, 6596–6605.
27 A.-C. Genix and J. Oberdisse, *Curr. Opin. Colloid Interface Sci.*, 2015, **20**, 293–303.
28 A. Meyer, R. Dimeo, P. Gehring and D. Neumann, *Rev. Sci. Instrum.*, 2003, **74**, 2759–2777.
29 R. T. Azuah, L. R. Kneller, Y. Qiu, P. L. Tregenna-Piggott, C. M. Brown, J. R. Copley and R. M. Dimeo, *J. Res. Natl. Inst. Stand. Technol.*, 2009, **114**, 341–358.
30 E. Senses, S. M. Ansar, C. L. Kitchens, Y. Mao, S. Narayanan, B. Natarajan and A. Faraone, *Phys. Rev. Lett.*, 2017, **118**, 147801.
31 K. Niedzwiedz, A. Wischnewski, M. Monkenbusch, D. Richter, A.-C. Genix, A. Arbe, J. Colmenero, M. Strauch and E. Straube, *Phys. Rev. Lett.*, 2007, **98**, 168301.
32 M. Brodeck, F. Alvarez, A. Arbe, F. Juranyi, T. Unruh, O. Holderer, J. Colmenero and D. Richter, *J. Chem. Phys.*, 2009, **130**, 094908.
33 D. Richter, M. Monkenbusch, A. Arbe and J. Colmenero, *Neutron Spin Echo in Polymer Systems*, 2005, pp. 1–221.

34 K. Niedzwiedz, A. Wischnewski, W. Pyckhout-Hintzen, J. Allgaier, D. Richter and A. Faraone, *Macromolecules*, 2008, **41**, 4866–4872.
35 A. P. Holt, P. J. Griffin, V. Bocharova, A. L. Agapov, A. E. Imel, M. D. Dadmun, J. R. Sangoro and A. P. Sokolov, *Macromolecules*, 2014, **47**, 1837–1843.
36 T. Glomann, G. Schneider, J. Allgaier, A. Radulescu, W. Lohstroh, B. Farago and D. Richter, *Phys. Rev. Lett.*, 2013, **110**, 178001.
37 A. Subbotin, A. Semenov, E. Manias, G. Hadziioannou and G. Ten Brinke, *Macromolecules*, 1995, **28**, 1511–1515.
38 A. Subbotin, A. Semenov, G. Hadziioannou and G. Ten Brinke, *Macromolecules*, 1995, **28**, 3901–3903.
39 P.-G. de Gennes, *J. Chem. Phys.*, 1971, **55**, 572.
40 A. Arbe, J. A. Pomposo, I. Asenjo-Sanz, D. Bhowmik, O. Ivanova, J. Kohlbrecher and J. Colmenero, *Macromolecules*, 2016, **49**, 2354–2364.
41 K. Niedzwiedz, A. Wischnewski, W. Pyckhout-Hintzen, J. Allgaier, D. Richter and A. Faraone, *Macromolecules*, 2008, **41**, 4866–4872.
42 K. Nusser, S. Neueder, G. J. Schneider, M. Meyer, W. Pyckhout-Hintzen, L. Willner, A. Radulescu and D. Richter, *Macromolecules*, 2010, **43**, 9837–9847.
43 Y. Li, M. Kröger and W. K. Liu, *Phys. Rev. Lett.*, 2012, **109**, 118001.
44 M. D. Vo and D. V. Papavassiliou, *Carbon*, 2016, **100**, 291–301.
45 L. Miao, H. Guo and M. J. Zuckermann, *Macromolecules*, 1996, **29**, 2289–2297.
46 G.-L. He, R. Messina and H. Löwen, *J. Chem. Phys.*, 2010, **132**, 124903.
47 S. Liu, E. Senses, Y. Jiao, S. Narayanan and P. Akcora, *ACS Macro Lett.*, 2016, **5**, 569–573.
48 H. Guo, G. Bourret, M. K. Corbierre, S. Rucareanu, R. B. Lennox, K. Laaziri, L. Piche, M. Sutton, J. L. Harden and R. L. Leheny, *Phys. Rev. Lett.*, 2009, **102**, 075702.
49 H. Guo, G. Bourret, R. B. Lennox, M. Sutton, J. L. Harden and R. L. Leheny, *Phys. Rev. Lett.*, 2012, **109**, 055901.
50 A. Kandar, J. Basu, S. Narayanan and A. Sandy, *Soft Matter*, 2012, **8**, 10055–10060.
51 R. Mangal, Y. H. Wen, S. Choudhury and L. A. Archer, *Macromolecules*, 2016, **49**, 5202–5212.
52 E. Senses and P. Akcora, *RSC Adv.*, 2014, **4**, 49628–49634.
53 N. Jouault, J. F. Moll, D. Meng, K. Windsor, S. Ramcharan, C. Kearney and S. K. Kumar, *ACS Macro Lett.*, 2013, **2**, 371–374.